Endothelial Cell-Anchored Tissue Factor Pathway Inhibitor Regulates Tumor Metastasis to the Lung in Mice

Jiping Wang,[1] Jiajun Xiao,[1] Danping Wen,[1] Xie Wu,[1] Zuohua Mao,[2] Jin Zhang,[1]* and Duan Ma[1,3]*

[1]Key Laboratory of Metabolism and Molecular Medicine, Ministry of Education, Department of Biochemistry and Molecular Biology, Institute of Biomedical Sciences, School of Basic Medical Sciences, Collaborative Innovation Center of Genetics and Development, Fudan University, Shanghai, China
[2]Department of Parasitology and Microbiology, Shanghai Medical College, Fudan University, Shanghai, China
[3]Children's Hospital, Fudan University, Shanghai, China

Tissue factor pathway inhibitor (TFPI) is a physiological inhibitor of the tissue factor (TF)-initiated coagulation pathway. Both circulating and tumor cell-associated TFPI significantly reduce tumor cell-induced coagulation activation and lung metastasis. However, the significance of endothelial cell-anchored TFPI in cancer biology remains largely unexplored. We generated mice with full-length disruption of TFPI (including TFPIα and TFPIβ isoforms) in endothelial cells, using a Cre-LoxP system and gene inactivation (GI) strategy. Experimental pulmonary tumor metastasis models were used with TFPI-deficient mice to evaluate the role of endothelial cell-anchored TFPI in cancer progression. Finally, lung microvascular permeability and microenvironment were investigated. TFPI-deficient mice were viable and fertile, and showed decreased plasma TFPI levels and lung TFPI levels as compared with their control littermates. TFPI deficiency in endothelial cells promoted pulmonary tumor metastasis with an increased vascular permeability and altered lung microenvironment. Our observations suggest that endothelial cell-anchored TFPI controls lung tumor metastasis, and does so largely through the inhibition of local TF-induced thrombin generation and the regulation of the lung microenvironment in mice. © 2015 Wiley Periodicals, Inc.

Key words: TFPI; conditional knockout; tumor metastasis; microvascular permeability; lung microenvironment

INTRODUCTION

Tissue factor pathway inhibitor (TFPI) is the natural inhibitor of the tissue factor (TF) coagulant pathway, and contains an acidic amino terminus, three tandem Kunitz-type domains (KD1, KD2, KD3), and a highly basic, positively charged carboxyl terminus (C terminus) [1]. The KD1 binds and inhibits the TF/VIIa complex, and the KD2 binds and inhibits factor Xa. The KD3 domain is not involved in the protease inhibitory activity, but coupling with protein S directly helps the TF-independent inhibitory effect of factor Xa by TFPI [2–4]. The C terminus is responsible for cell membrane anchoring [5,6]. Furthermore, the functions of TFPI extend beyond its anti-coagulant role, and participate in different aspects of vascular biology. TFPI interferes with endothelial cell migration in a TF-independent manner [7]. The C terminus independently displays anti-inflammatory, anti-angiogenic, and anti-tumor properties [8,9]. The functional importance of TFPI is confirmed in that no human subject or patient with TFPI deficiency has been identified. Systemic homozygotic deletion of KD1 of the *TFPI* gene results in intrauterine lethality in mice [10,11].

The dominant source of TFPI is thought to be the microvascular endothelium. The two main isoforms of TFPI, TFPIα and TFPIβ, have been reported, which differ in their domain structure, manner for cell surface attachment and more importantly, in potential function. Approximately, 95% of mature TFPI produced by endothelial cells remains at the cell surface as a glycosyl-phosphatidylinositol (GPI)-anchored protein with a small portion (TFPIα) released into the plasma (70 ng/ml) [6,12,13]. The localization of TFPI expression and its role in development highlights the physiological importance of anchored TFPI, suggesting that TFPI anchoring contributes to the integrity of the vascular endothelia or the microvasculature [14,15].

The hemostatic components and cancer cells are inter-crossed in multiple ways. While hemostatic factors play a role in tumor progression, cancer cells can activate the coagulation system. TF is the primary cellular initiator of blood coagulation and is a

modulator of angiogenesis and metastasis in cancer. Studies have shown that TF is highly expressed in many tumor cell types, including glioma, non-small cell lung cancer, pancreatic cancer, colorectal cancer, and ovarian cancer [16–20] and is involved in tumor-associated hypercoagulability, and in promoting tumor angiogenesis and metastasis. The level of TF expression in tumor tissues correlates with histological grade of the malignancy and vascularity [21]. TFPI is involved in cancer biology through both TF-dependent and TF-independent pathways [8,22]. Studies show that over-expression of TFPI in breast cancer cell-lines induces apoptosis, whereas down-regulation of TFPI was associated with increased self-sustained cell growth [23,24]. It has previously been reported that intravenous injection of recombinant TFPI resulted in reduced metastasis in murine models [25]. TFPI is also expressed in breast, pancreatic, and colorectal cancer cells, suggesting that in the tumor microenvironment, TFPI may facilitate the growth of tumor cells or prevent intra-tumor vessel auto-coagulation [26,27]. However, no direct data are available regarding the physiological roles of endothelial-anchored TFPI in cancer biology.

To further determine the physiological role of endothelial anchored TFPI, we used the Cre-Loxp system and a gene inactivation strategy to generate mice with the full-length TFPI knockout (including TFPIα and TFPIβ, and theoretical expression of only 99 bp of exon 2 encoding the signal peptide and N terminus domains). Our data showed that TFPI conditional knockout (CKO) in murine endothelial cells resulted in defects of vascular endothelia in the lung, which promoted pulmonary metastasis.

MATERIALS AND METHODS

Generation of Floxed TFPI Mice

The Institutional Animal Care and Use Committee of Fudan University, China approved all protocols. Conditional knockout of TFPI in a cell type-specific manner was accomplished using a Cre recombinase-mediated unidirectional DNA inversion strategy [28]. Insertion of a reversed "flipflox" vector, consisting of a gene inactivation cassette (GI) and an internal ribosome entry site (IRES)-GFP reporter, into intron 3 of TFPI, was transcriptionally silent and did not affect TFPI expression. Crossing with ubiquitous or lineage-specific Cre recombinase permanently inverted the inserted GI cassette and blocked full-length TFPI transcription (Figure 1A). A conditional targeting vector (pDualve) was used, and two homologous arms were obtained by homologous recombination in bacteria [29]. The final targeting vector contained the 5′arm (5012 bp), the 3′arm (3520 bp), and the GI cassette (2584 bp), which was flanked by two mutant loxP (mloxP) sites [30], a Frt floxed neo-positive selection cassette (3520 bp) and a thymidine kinase (TK)-negative selection cassette (5810 bp).

The construct was linearized and electroporated into SCR012 PluriStem 129/S6 murine ES cells. Clones carrying the construct were identified by long range PCR (LR-PCR) after positive and negative selection. The set of primers were P1, 5′-GGGCCGCAGAGAT-GACTAGGCTGTTA-3′; P2, 5′-TCGATCCTCTA-GAGCGGCCATCATAA-3′ for the 5′arm; and P3, 5′-CTGAGCCCAGAAAGCGAAGGA-3′; P4, 5′-GGCCAA-TTATTGTTAACTTATCC-3′ for the 3′arm (Figure 1B).

Removal of the pGK-NEO cassette was accomplished by crossing the homozygous TFPI floxed (TFPI$^{fl/fl}$) mice with the neo selection cassette, and 129S4/SvJaeSor-Gt (ROSA) 26Sor$^{tm1(FLP1)\ Dym}$/J (Jackson Laboratory, Bar Harbor, ME). The resulting TFPI$^{fl/+}$ mice were serially backcrossed to the C57BL/6J strain for four generations (F4), and intercrosses of these F4 animals were used in subsequent experiments. The following sets of primers were used for analysis of Neo and FLP sequences: Neo-F, 5′-AATGCTCTTTGGAGGCCATGATTCAG-3′; Neo-R, 5′-TGACTAGGCCATCTGATACA-3′; FLP-F, 5′-CACT-GATATTGTAAGTAGTTTGC-3′, and FLP-R, 5′-CTAGTGCGAAGTAGTGATCAGG-3′. All these procedures were carried out in Shanghai Biomodel Organism Science & Technology Development Co.,Ltd.

Generation of Mice With a TFPI Conditional Knockout

To generate mice with an endothelial-specific disruption of TFPI, homozygous TFPI floxed mice were crossed with B6.Cg-Tg(Tek-cre) 12Flv/J mice (Tek-Cre) that were obtained from The Jackson Laboratory [31,32]. The resulting offspring were backcrossed to TFPI floxed homozygosity and maintained the Tek-Cre transgene.

RT-PCR to Determine TFPI Transcriptional Silencing

The identification of TFPI transcriptional silencing was performed by RT-PCR using three primers:P8, 5′-TCTGTTGCTTAGCCTTGTTCCCGAGTT-3′; P9, 5′-GA-CAAACGCACACCGGCCTTATTCCAA-3′; P10, 5′-AG GCCGGTGTTCTTCAGGATCTGCTTG-3′ (Figure 1C). P8 was in Exon 3, while P9 and P10 were in the sequences of IRES and GFP, respectively. These primers were intentionally designed to determine whether TFPI mRNA was transcriptionally silent.

PCR Genotyping of Targeted Mice

Three primers were used for genotyping the offspring: P5, 5′-TCTTCCTGTTGTCTGGGACATCCTG-3′; P6, 5′-AATGCTCTTTGGAGGCCATGATTCAG-3′; P7, 5′-GCCAGACACCTTTAATCCCAGCAC-3′. Both P5 and P7 were in intron 3, while P6 was in the GI cassette. The set of primers was used to determine whether the GI cassette existed or not. To detect the Tek-cre transgene, we used the primers: Tek-cre-F, 5′-GGCTGTGGAATCGGTCTCTAGTGGC, and Tek-cre-R, 5′-CGAACATCTTCAGGTTCTGCGGGAAA-3′ (Figure 1D).
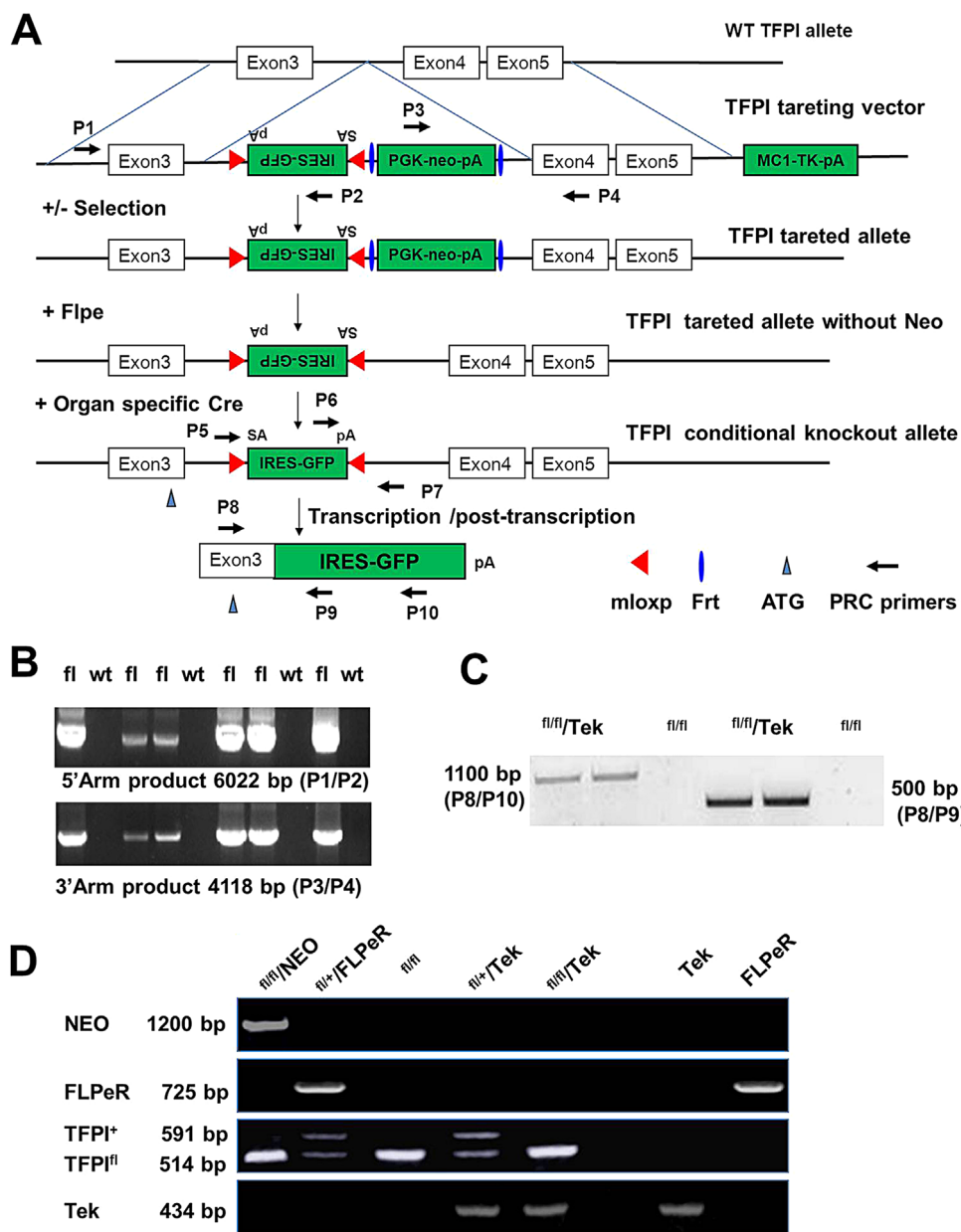
Figure 1. TFPI conditional knockout strategy and genotyping. (A) The final targeting vector contains a 5′arm, a 3′arm, and a GI cassette flanked by two mutant loxP (mloxP) sites, and a Frt floxed neo-positive selection cassette and a thymidine kinase (TK)-negative selection cassette. The targeting vector was linearized and electroporated into SCR012 PluriStem 129/S6 Murine ES cells. After deletion of PGK-neo by breeding TFPI^fl mice with FRT mice, TFPI^fl/fl mice were crossed with lineage-specific Cre recombinase, which led to a permanently inverted GI cassette and blocking of the full-length TFPI expression. (B) Targeted 129/S6 murine ES cells and founders were identified by using long-range PCR. (C) RT-PCR was used to determine transcriptional silencing of TFPI. (D) PCR genotyping of the offspring derived from crossing TFPI^fl/fl mice with FRT mice or TFPI^fl/+/Tek mice.

Quantitative Real-Time PCR (qPCR)

To analyze the gene expression levels, total RNA of different tissues was isolated using the RNeasy fibrous tissue mini kit (Qiagen, Germantown, MD), and cDNA was synthesized using reverse transcriptase (Takara, Tokyo, Japan). qPCR was conducted using SYBR green (Applied Biosystems, Darmstadt, Germany). The data were collected using the ABI7500 system (Applied Biosystems). Result analyses were performed using the $2^{-\triangle\triangle CT}$ Method. Primers of TFPI (designed for transcript 1, NM_011576.1, and transcript 2, NM_001177319.1) and GAPDH (endogenous control) are as follows: TFPI-F, 5′-TCTGTTGCTTAGCCTTGTTCCCGA-3′, and TFPI-R, 5′-TGCTTTGCATGGACCATCATCTGC-3′; GAPDH-F, 5′-TGTCGTGGAGTCTACTGGTGTCTT-3′, and GAPDH-R, 5′-TTCTCGTGGTTCACACCCATCACA-3′. All qPCR primers in this study were listed in the supplementary Table 1.

Enzyme-Linked Immunosorbent Assay (ELISA)

Blood was collected via cheek pouch puncture into a tube containing 0.1 M sodium citrate (one-tenth the volume of blood collected), which was centrifuged at 8000g for 15 min at 4°C, and the resulting plasma was isolated and frozen at −80°C until analysis. Plasma concentrations of TFPI (E0394Mu; USCN Life Science, Wuhan, Hubei, PRC) and thrombin-antithrombin (TAT) complex (KA1857; Abnova, Taipei City, Taiwan) were measured using ELISA assay kits following the manufacturer's instructions.

Blood Analysis

Plasma specimens were analyzed within 2 h of collection for prothrombin time (PT), thrombin time (TT), activated partial thrombin time (APTT). Sysmex CA1500 (Sysmex Corporation, Kobe, Japan) was used for this analysis according to the manufacturer's protocols.

Western Blotting

Mouse lungs were homogenized in 1 ml RIPA buffer (Cell Signal, Beverly, MA) containing complete proteinase inhibitor cocktail (Roche Diagnostics, Basel, Switzerland) and protein concentrations were measured using the Bio-Rad Bradford protein assay (Bio-Rad, Hercules, CA). Signals were detected with rabbit polyclonal anti-TFPI (sc-28862; 1:1000; Santa Cruz Biotechnology, Santa Cruz, CA) overnight at 4°C, followed by incubation with the appropriate secondary antibody. An ECLTM Western blot analysis system (GE Healthcare Life Sciences, Pittsburgh, PA) was used to detect the bands according to the protocols. Densitometry was done, and normalized to β-tubulin protein expression levels.

Experimental Pulmonary Tumor Metastasis

Groups of five mice with different genotypes were inoculated with 1×10^5 B16 melanoma cells (ATCC) via the tail vein. Then, 12–14 d later, the lungs were removed, and the number of pulmonary colonies was counted under a dissecting microscope [33]. Groups of five mice with different genotypes were injected s.c. into the left flanks with 1×10^6 Lewis lung carcinoma cells (LLC, ATCC). These s.c. tumors were removed surgically 3 wk after the tumor implantation, when the size of the tumors reached 1–1.5 cm in the longest diameter. Three weeks after surgical removal of the s.c. tumors, the mice were sacrificed, and their lung tissues were examined. Pulmonary metastatic burden was assessed by counting surface pulmonary tumors under a dissecting microscope [34].

Plasma TAT, Fibrinogen Levels, and Platelet Count Before and After B16 Melanoma Cell Injection

Six- to eight-wk-old TFPI$^{fl/fl}$/Tek mice and TFPI$^{fl/fl}$ were randomly appointed to three groups, respectively ($n = 5$–6 in each group). Plasma TAT, fibrinogen levels, and platelet count before (0 h) and after B16 melanoma cell injection (1 and 2 h) were determined. Plasma concentrations of thrombin-antithrombin (TAT) complex were measured using ELISA assay kits following the manufacturer's instructions. Sysmex CA1500 (Sysmex Corporation, Kobe, Japan) was used for analysis of plasma fibrinogen according to the manufacturer's protocols. Platelet counts were analyzed utilizing automated hematology analyzers (LH 780; Beckman Coulter, CA).

Adenovirus Infection

The recombinant adenovirus AdTFPI (AH806099; ViGene Biosciences, Inc., Rockville, MD), expressing TFPI, was used to recover the expression of TFPI, with Green fluorescent protein (GFP)-expressing adenovirus, AdGFP (ViGene Biosciences, Inc.) as the negative control. Six- to eight-wk-old TFPI$^{fl/fl}$/Tek mice were randomly appointed to three groups: Group 1 ($n = 6$) was mock infected with 1×10^9 infective units (IFU) of AdGFP per mouse in 200 of saline by intravenous injection into the tail vein. Group 2 ($n = 6$) and Group 3 ($n = 7$) received the same IFU of AdTFPI. Three days later, all groups were inoculated with 1.5×10^5 B16 melanoma cells via the tail vein. Group 1 and Group 2 were treated with AdGFP and Group 3 with AdTFPI at 4 days postinjection (dpi). All the mice were sacrificed and the lung samples were collected at 16 dpi. The number of pulmonary colonies was counted under a dissecting microscope. Tumor and lung tissues were harvested from each group for HE staining. In addition, we examined the expression of AdGFP and AdTFPI of B16 melanoma cells in culture (see supplementary Figure S5).

Evans Blue Microvascular Permeability

Pulmonary microvascular permeability was measured using a modification of the Evan's blue dye extravasation technique [35].

Transmission Electron Microscopy (TEM)

TEM of lung tissues was performed according to routine procedures. Briefly, the tissues were fixed (2.5% glutaraldehyde + 3% paraformaldehyde) in 0.1 M PB (pH 7.4), and then washed three times in 0.1 M PB and post-fixed in 1% OsO$_4$, followed by washing with 0.1 M sodium cacodylate and then distilled-deionized water. The tissues were then dehydrated by sequential washings in 25%, 50%, 75%, and 100% ethanol, and then embedded in epon 812 (Electron Microscopic Sciences, Fort Washington, PA). The ultrathin sections (70 nm) were stained with uranyl acetate and lead citrate and examined with a TEM (JEM-1200EX, Tokyo, Japan).

Immunohistochemistry

Dissected lungs were fixed in 4% paraformaldehyde (PFA) in PBS overnight at 4°C and then embedded in paraffin. Next, 4–6 μm thick sections were cut and

processed for immunohistochemical analysis. Antigen retrieval was performed on paraffin-embedded sections by heating in pH 6.0 citrate buffer for 20 min. The primary antibodies for TFPI (sc-18712; 1:100; Santa Cruz Biotechnology, Santa Cruz, CA), TF (sc-23596; 1:100; Santa Cruz Biotechnology), TFPI-2 (#186747; 1:200; Abcam, Cambridge, MA), VEGF (AF-493-NA; 1:250; R&D Systems, CA), VEGFR2 (#14-5821-82; 1:200; eBioscience, San Diego, CA), were used for 30 min, and the secondary antibody and DAB staining kit were used as described in the product manual (DAKO Cytomation, Carpinteria, CA). Images of four representative fields were captured and integrated optical density (IOD) (pixels) was measured by Image-Pro v6.0 software (Media Cybernetics, Bethesda, MD).

Statistical Analysis

All experimental values are presented as the mean $\pm$ SEM. Statistical significance of the data was determined by the two-tailed Student's *t*-test. A *P*-value of <0.05 was considered significant.

RESULTS

Generation of Mice With Endothelial-Specific Disruption of TFPI

Traditional and conditional knockout methods have been utilized to generation of mice with the *TFPI* gene deletion. Two kinds of TFPI knockouts have been reported [10,11]. However, both of them have only deleted Kunize Domain 1 (KD1), which leads to a TFPI protein without KD1, but with KD2, KD3, and the C terminus domains intact, which are normally expressed and functional on the surface of endothelial cells.

To elucidate the physiological function of TFPI that is located on the surface of vascular endothelia, we designed and generated mice with full-length TFPI knockout using the Cre/loxP system and gene inactivation (GI) strategy. The system uses two mutant loxP sites and when Cre recombinase is present, the inserted GI cassette will be inverted. Therefore, this generates a disrupted TFPI transcript that only contains the sequence of the exon 2 that encodes the signal peptide and N-terminal domain, which is 33 amino acids and expresses the GFP from an inserted GI cassette (Figure 1A).

Targeted 129/S6 murine ES cells and founders were screened and determined by long-range PCR (LR-PCR) using primers P1, P2, P3, and P4. The PCR products of the 3′ and 5′ arms were 4118 bp, and 6022 bp, respectively (Figure 1B). Four chimeric male mice derived from the microinjected mouse blastocysts successfully transmitted the mutation to the germline. These mice provided founders for subsequent inbreeding. The NEO selection marker were deleted after two generation crossing with mice (129S4/SvJaeSor-Gt(ROSA) 26Sor[tm1(FLP1) Dym]/J).

To demonstrate the efficiency of the *Cre-loxP* gene targeting system for the TFPI knockout, TFPI floxed mice were crossed with FVB/N-TgN(EIIa-cre) C5379Lmgd/J that constitutively expressed Cre recombinase. All homozygous embryos carrying the Cre transgene led to intrauterine lethality (see supplementary Figure S1) as reported, which suggests that the knockout strategy used in the present study is effective.

As mentioned above, the knockout strategy applies the inversion of the GI cassette flanked by two loxPs. We analyzed the efficiency of inversion by crossing TFPI flox mice (TFPI[fl]) with Cre transgenic mice (Tek-Cre, Nestin-Cre, SMA-Cre; data no shown). All TFPI^{fl/+} or TFPI^{fl/fl} carrying the Cre transgene produced an inversion of the GI cassette. To determine whether the TFPI mRNA was trapped, we used RT-PCR to analyze the mutant transcript (Figure 1C). Endothelial TFPI conditional knockout was achieved by crossing the TFPI[fl] mice with transgenic mice expressing Cre recombinase under the control of the Tie2 promoter/enhancer (Tek-Cre). Genotyping of the offspring was determined by PCR (Figure 1D). Mice were indistinguishable from their normal littermates. Endothelial TFPI conditional knockouts were alive and fertile.

Efficiency of TFPI Knockout in Organs and the Plasma

To evaluate the efficiency of TFPI knockout in various organs, TFPI mRNA was determined by qPCR using wild-type TFPI primers. TFPI mRNA levels (containning both transcript 1 and transcript 2) in the lung, spleen, heart, kidney, liver, and the brain of TFPI^{fl/fl}/Tek mice were $30.3\% \pm 4.5\%$ ($P = 0.0005$), $18.8\% \pm 1.7\%$ ($P = 0.0001$), $48\% \pm 8.3\%$ ($P = 0.0053$), $41.6\% \pm 4.1\%$ ($P = 0.0479$), $58.7\% \pm 3.6\%$ ($P = 0.0352$), and $46\% \pm 13\%$ ($P = 0.0456$) of that of their TFPI^{fl/fl} littermates (Figure 2A), respectively. To investigate whether TFPI decreased accordingly in the plasma, we determined TFPI concentrations in plasma by ELISA. Plasma TFPI concentrations of TFPI^{fl/fl}/Tek mice were $40.2\% \pm 1.2\%$ lower ($P = 0.0006$) than that of their TFPI^{fl/fl} littermates (Figure 2B). Expression of the TFPI protein in the lung was analyzed by Western blotting, which showed that TFPI protein was $54\% \pm 8.1\%$ of that of control mice ($P = 0.0107$, Figure 2C).

Blood Analysis

Prothrombin time (PT), thrombin time (TT), activated partial thrombin time (APTT) were analyzed using Sysmex CA1500. The results showed that PT, TT, and APTT had no significant difference ($P > 0.05$) between TFPI^{fl/fl}/Tek mice and their TFPI^{fl/fl} littermates (data no shown). In addition, we used the tail-bleeding time to evaluate hemostasis in TFPI^{fl/fl}/Tek mice and their TFPI^{fl/fl} littermates; but there was no significant difference here (data no shown). Baseline plasma TAT, fibrinogen levels, and platelet counts were also evaluated for the TFPI-deficient and control mice (See Results section and Figure 4)
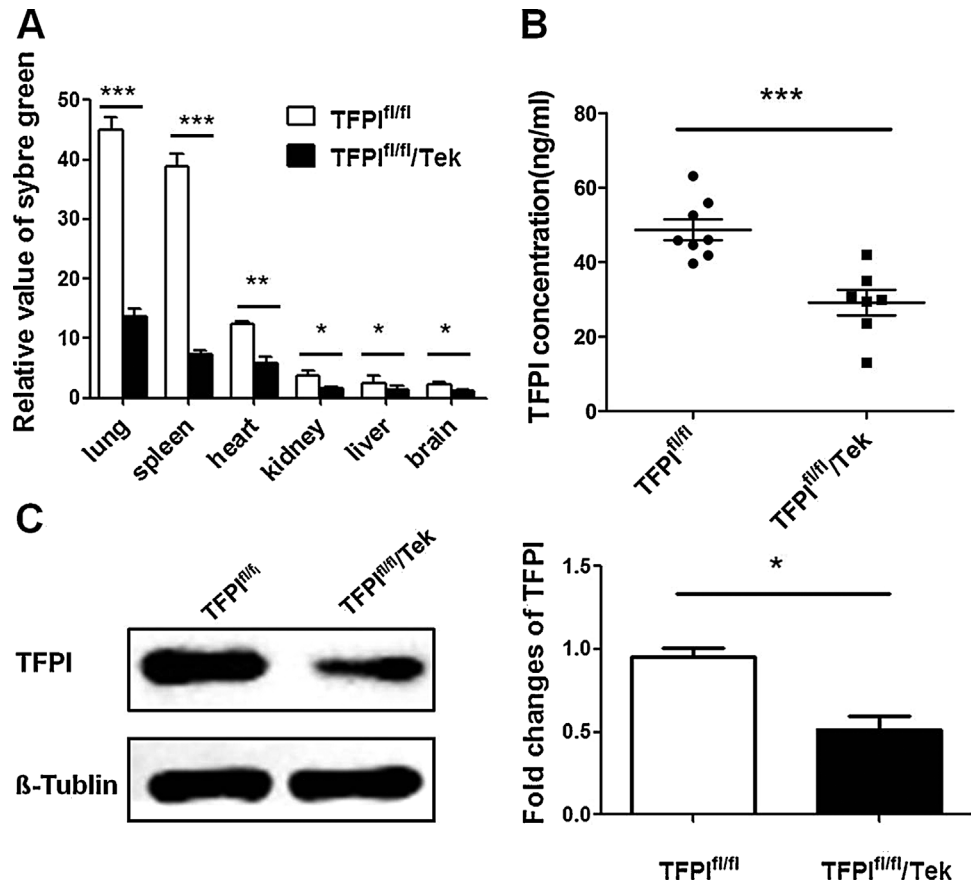
A

B

C

Figure 2. Decreased TFPI expression in organs and circulating TFPI in TFPI-deficient murine plasma. (A) Detection of TFPI mRNA levels by qPCR. Total RNA that was isolated from mouse lung, spleen, heart, liver, kidney, and cerebrum was subjected to qPCR analysis. TFPI mRNA levels in the lung, spleen, heart, kidney, liver, and brain of TFPI$^{fl/fl}$/Tek mice were 30.3%, 18.8%, 48%, 41.6%, 58.7%, 46% of that of their TFPI$^{fl/fl}$ littermate counterparts. Data are representative of three independent experiments. (B) The plasma TFPI concentration of TFPI$^{fl/fl}$/Tek mice ($n = 7$) by ELSIA was 40.2% lower than that of their TFPI$^{fl/fl}$ littermates ($n = 8$). (C) Detection of TFPI protein by immunoblotting in the mouse lung. The intensity of the bands was quantified by densitometry. Data are representative of three independent experiments. $^{*}P < 0.05$; $^{**}P < 0.01'$; $^{***}P < 0.001$. Error bars indicate SEM.

Endothelial-Specific TFPI Deficiency Exhibits Enhanced Pulmonary Tumor Metastasis

To directly test the hypothesis that anchored TFPI is an important determinant of metastatic potential, we used two models of experimental pulmonary tumor metastasis: i.e., models of B16 melanoma cells via the tail-vein, and LLC via s.c. administration. Within 12–14 d of B16 challenge, all three groups of mice appeared active and overtly healthy. After sacrifice, gross examination of the organs revealed multiple organ metastases, including in the lung, heart, liver, and the kidney, and yet there was no evidence of a significant difference except in terms of the numbers of tumor clones in the lungs (Figure 3A, B). The numbers of B16 tumor clones of TFPI$^{fl/fl}$/Tek mice was 4.8-fold higher than that of TFPI$^{fl/+}$/Tek ($P < 0.0001$), and was 5.6-fold higher than that of TFPI$^{fl/fl}$ mice ($P = 0.001$; Figure 3C). This dramatic increase in metastatic potential conferred by TFPI deficiency was not limited solely to B16 melanoma cells. In the Lewis lung murine tumor model, the control mice and heterozygous CKO mice appeared to be healthy 3 wk after surgical removal of the s.c. tumors, whereas most of the homozygous CKO mice became distinctly sick. LLC clones of pulmonary tumor metastases were confluent in the lungs of TFPI$^{fl/fl}$/Tek mice (Figure 3D, E). The results showed that the number of LLC clones of TFPI$^{fl/fl}$/Tek mice was 13.1-fold higher than that of TFPI$^{fl/+}$/Tek mice and 18.8-folds higher than that of TFPI$^{fl/fl}$ (both at $P < 0.0001$; Figure 3F). The data derived from both mouse tumor metastases models indicated that TFPI deficiency facilitated pulmonary tumor metastasis through hematogenous metastasis or the primary tumor. In addition, our observation on the primary tumor growth of B16 and LLC suggests that TFPI deficiency did not enhance the growth of the tumor (data not shown).

Plasma TAT, Fibrinogen Levels, and Platelet Count Before and After B16 Melanoma Cell Injection

To investigate the tumor cell-induced coagulopathy, TAT, Fibrinogen, and platelet were examined before and after tumor cell injection in endothelial TFPI-deficient

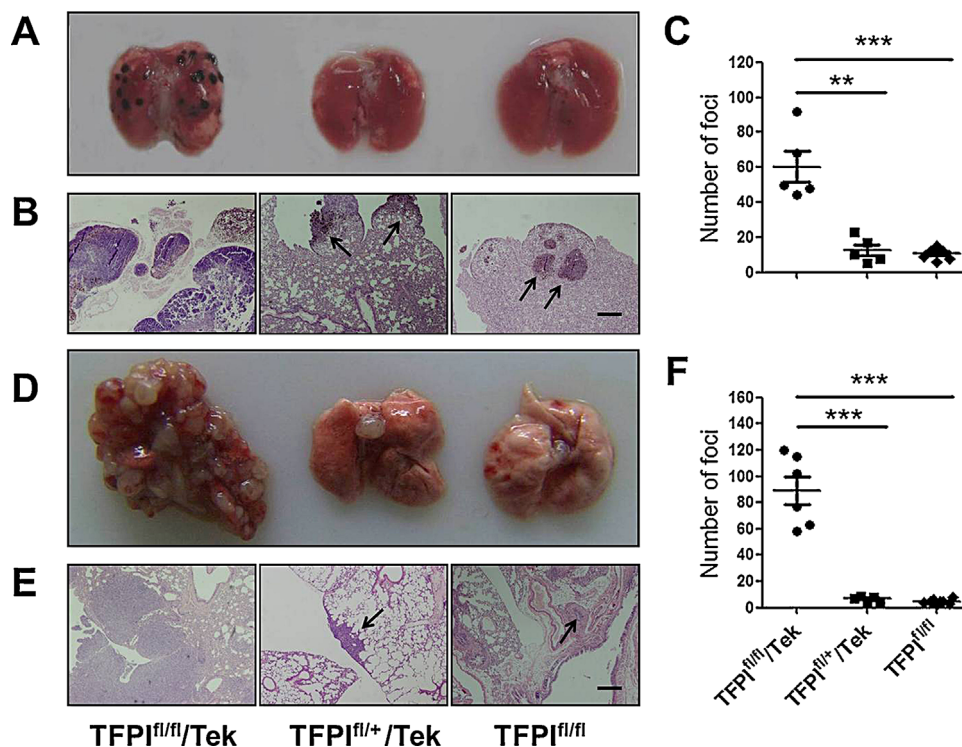**TFPI$^{fl/fl}$/Tek** **TFPI$^{fl/+}$/Tek** **TFPI$^{fl/fl}$**

Figure 3. TFPI deficiency in mice enhances tumor metastasis to the lung. (A) Representative lungs with B16 metastases at 12–14 d after intravenous administration of tumor cells. (B) HE stained sections of lung tissue revealed small metastatic foci (arrow) in the lungs of TFPI$^{fl/+}$/Tek mice ($n=5$) and TFPI$^{fl/fl}$ ($n=7$); whereas lungs that were harvested from TFPI$^{fl/fl}$/Tek mice ($n=5$) were largely effaced by tumor tissue. (C) The number of surface pulmonary tumors was counted in lung tissues. The number of tumor foci between TFPI$^{fl/fl}$/Tek mice and TFPI$^{fl/+}$/Tek mice and TFPI$^{fl/fl}$ were shown. (D) Representative images of LLC clones of pulmonary tumor metastasis of three genotyped mice. (E) HE sections showed largely involved lung tissues that were harvested form TFPI$^{fl/fl}$/Tek mice. (F) The counting results were shown between TFPI$^{fl/fl}$/Tek mice ($n=6$), TFPI$^{fl/+}$/Tek mice ($n=5$), and TFPI$^{fl/fl}$ mice ($n=8$). Arrow indicates tumor foci. $^{**}P<0.01$; $^{***}P<0.001$. Scale bar $=200\,\mu$m. Error bars indicate SEM in (C, F).

mice and control mice. TAT plasma levels increased from 6.08 ± 0.7 ng/ml before injection to 17.5 ± 2.27 ng/ml at 2 h after tumor cell injection in control mice. In TFPI$^{fl/fl}$/Tek mice, the increase was more pronounced from 8.6 ± 2 ng/ml before injection to 23.64 ± 2.46 at 2 h after tumor cell injection. Endothelial TFPI deficiency mice demonstrated significantly higher levels of TAT compared with control mice before tumor cell injection ($P=0.025$) and at 2 h after tumor cell injection ($P=0.0035$; Figure 4A). In contrast, Fibrinogen plasma levels were significantly lower in TFPI$^{fl/fl}$/Tek mice than in control mice (Figure 4B). The fibrinogen plasma level at 0 h before tumor cell injection was 1.2 ± 0.19 g/L in the TFPI$^{fl/fl}$/Tek group compared with 1.7 ± 0.27 g/L in the TFPI$^{fl/fl}$ group ($P=0.0103$). After tumor cell injection, the fibrinogen plasma level at 2 h was 0.36 ± 0.13 g/L in the TFPI$^{fl/fl}$/Tek group compared with 0.69 ± 0.12 g/L in the TFPI$^{fl/fl}$ group ($P=0.0024$). As shown in Figure 4C, platelet counts dropped from $1226 \pm 69 \times 10^9$/L at 0 h to $866 \pm 140 \times 10^9$/L at 2 h after the injection of B16 melanoma cells in control mice. In mice with an endothelial TFPI deficiency, the drop in platelet count
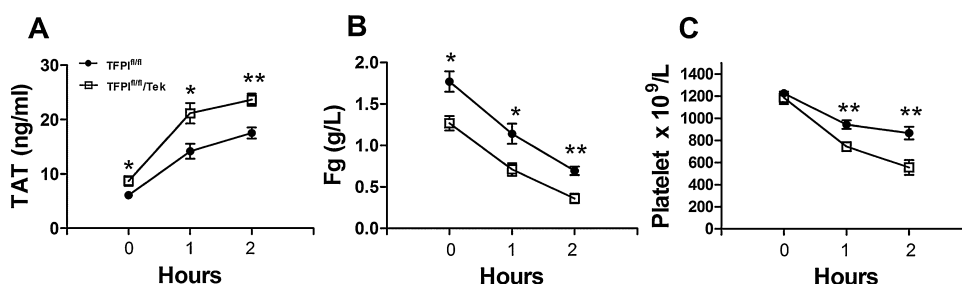

Figure 4. Plasma TAT, fibrinogen levels, and platelet count before and after B16 melanoma cell injection. TAT (A), fibrinogen concentration (B) and platelet count (C) were determined before (0 h) and after the injection of B16 melanoma cells (1 and 2 h) in TFPI$^{fl/fl}$/Tek and TFPI$^{fl/fl}$ mice ($n=5$–6 in each group). $^{*}P<0.05$; $^{**}P<0.01$; Error bars indicate SEM.

was significantly more profound, reaching levels as low as $555 \pm 163 \times 10^9$/L at 2 h after tumor cell injection ($P = 0.005$). These data suggest that endothelial-specific TFPI deficiency exacerbates tumor cell-induced coagulopathy in mice.

AdTFPI Administration Decreases Tumor Metastasis to the Lung

To evaluate the role of TFPI in suppressing metastasis, we used TFPI-expressing adenovirus in experimental lung metastasis model of B16 melanoma cells. Three groups of TFPI$^{fl/fl}$/Tek mice were pretreated with AdGFP or AdTFPI 3 d before the injection of B16 melanoma cells. Mice in Group 3 were administrated with AdTFPI the second time immediately after tumor cell injection. Pulmonary metastatic foci were examined 16 d later. Our results showed that AdTFPI administration decreases tumor metastasis to the lung in endothelial-specific TFPI deficiency mice. The reduction in tumor burden in mice of Group 2 and Group 3 (one treatment with AdTFPI for Group 2 and two treatments for Group 3) was statistically significant compared with that in mice receiving AdGFP ($P = 0.025$ and $P = 0.002$, respectively; Figure 5). These results suggest that TFPI has significant anti-metastatic activity and may do so by regulating tumor cell-induced TF-mediated coagulation activation.

TFPI Deficiency Results in Increased Microvascular Permeability

To determinate whether TFPI deficiency resulted in increased microvascular permeability, a modification of the Evans blue dye extravasation technique was used with or without LPS (Figure 6A, B, D, and E). Compared with their TFPI$^{fl/fl}$ littermates, Evans blue extravasation in the lungs of TFPI$^{fl/fl}$/Tek mice were $34\% \pm 6.7\%$ higher ($P = 0.0127$; Figure 6C) without LPS and 3.12-folds higher ($P = 0.0012$; Figure 6F)

when LPS was used simultaneously. There was not a significant difference in the brain among the groups without LPS (data not shown), but when LPS was used to challenge with Evans blue stain, the brain microvascular permeability of TFPI$^{fl/fl}$/Tek mice showed a 4.6-fold higher effect than that of TFPI$^{fl/fl}$ mice (see supplementary Figure S2). Our data indicate that the importance of TFPI is different in a given organ, and further demonstrates a tissue-specific mechanism in operation.

We further observed pulmonary microvascular endothelial cells by transmission electron microscope (TEM) for evaluation of the cell–cell junctional integrity. Cell–cell junctions of pulmonary endothelial cells in the lungs of TFPI$^{fl/fl}$ were tight, whereas there was increased gap between adjacent cells in the lungs of TFPI$^{fl/fl}$/Tek mice (Figure 7). About 16% (16/100) of the pulmonary endothelial cells of TFPI$^{fl/fl}$/Tek mice were swollen, and/or were adherent to platelets or neutrophilic granulocytes. In addition, the endothelial structure in mouse hearts was also analyzed by TEM. In three genotypic mice, TFPI deficiency had no significant effect on microvascular endothelial cells in the hearts, which indicated that a 52% decrease at the mRNA level was insufficient to change the integrity of endothelial cells (see supplementary Figure S3).

TFPI Deficiency Leads to Changes of the Pulmonary Microenvironment

We performed qPCR with lung tissue to examine the transcript levels for genes that were involved in tumor metastasis. Among the 16 genes (Figure 8) that we analyzed, eight of them showed a significant increase of more than twofold in the lung cDNA of TFPI$^{fl/fl}$/Tek mice, as compared with TFPI$^{fl/fl}$ mice. These genes included *TFPI-2* (3.6-fold), *VEGF* (4.3-fold), *Flk-1* (6.8-fold), *MMP-2* (2.2-fold), *collagen-1* (2.4-fold), *E-selectin* (threefold), *perlecan* (2.9-fold),
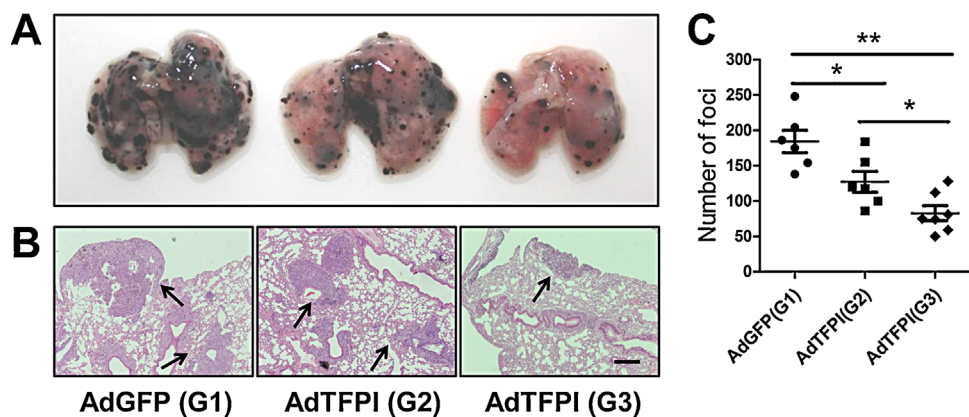

Figure 5. AdTFPI administration decreases tumor metastasis to the lung. (A) Representative photograph of pulmonary metastatic foci produced 16 d after intravenous injection of B16 melanoma cells and AdGFP and/or AdTFPI. The reduction in tumor burden in TFPI$^{fl/fl}$/Tek mice receiving AdTFPI (one treatment for Group 2, $n = 6$ and two treatments for Group 3, $n = 7$) was statistically significant compared with that in mice receiving AdGFP (Group 1, $n = 6$). (B) HE stained sections of lung tissue revealed metastatic foci (arrow) in the lungs. Scale bar = 200 μm. (C)
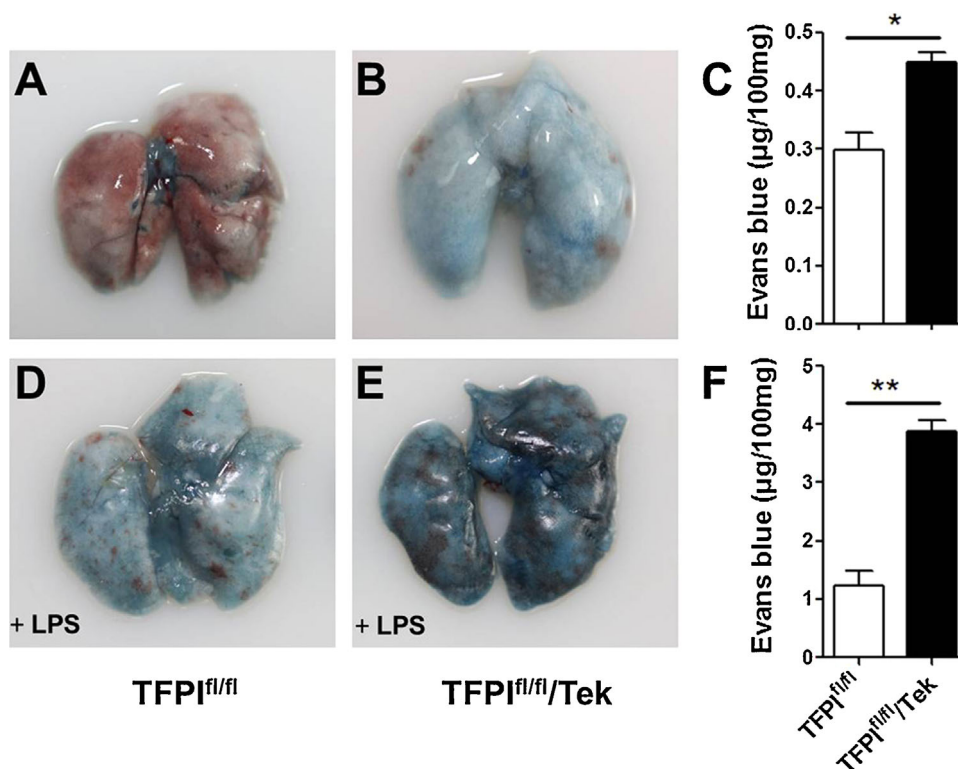
Figure 6. TFPI deficiency leads to increased pulmonary microvascular permeability. (A–C) Pulmonary microvascular permeability was measured using a modification of the Evans blue dye extravasation technique. Compared with their TFPI$^{fl/fl}$ littermates ($n = 5$), Evans blue extravasation of TFPI$^{fl/fl}$/Tek mice ($n = 5$) was 34% higher. (D–F) Pulmonary microvascular permeability was also evaluated by simultaneous administration of Evans blue stain, and LPS. Evans blue extravasation of TFPI$^{fl/fl}$/Tek mice ($n = 5$) was 3.12-fold higher than that of TFPI$^{fl/fl}$ littermates ($n = 5$). $^{*}P < 0.05$; $^{**}P < 0.01$. Error bars indicate SEM in (C, F).

and *Lama-5* (2.4-fold). Interestingly, at the mRNA level, TF seemed repressed. We confirmed the expression of TFPI, TF, TFPI-2, VEGF, and Flk-1 by immunohistochemistry. Our data showed that TFPI-2, VEGF, and Flk-1 were upregulated, while TF showed no significant difference in TFPI$^{fl/fl}$/Tek mice (Figure 9). The TFPI-2 protein in lung tissue increased about two- to threefold compared with control. Using the results of immunohistochemistry, the TF/TFPI balance was calculated. The ratio of TF/TFPI was 1.39 in lung tissue of TFPI deficiency mice if the ratio in control mice was 1. Upregulated VEGF-A, Flk-1, and MMP2 may offer a pulmonary microenvironment that facilitates tumor metastasis. The survival, migration, and proliferation of endothelial cells is regulated primarily by VEGF-A binding to VEGFR2 (Flk-1). Tumor cell-derived VEGF can bind to VEGFR2 on endothelial cells, thus, stimulating tumor vessel formation. In addition, other gene tested also play roles in cancer progress. E-selectin mediates the adhesion of tumor cells to endothelial cells, whereas perlecan is a potent inducer of tumor growth and angiogenesis. Collagen-1 can enhance the injury done to ECM by absorbing plasmin from the plasma. The upregulated TFPI-2, which is a homolog of TFPI, may be a compensative mechanism for TFPI

deficiency. TFPI-2 is involved in regulating pericellular proteases, a strong plasmin inhibitor, through which TFPI-2 prevents activation of MMPs. The phenomenon that TFPI deficiency in mice led to the repressed expression of TF, and accompanied the enhanced expression of TFPI-2 was also observed in mice with TFPI knockout in the smooth muscle cells, when the smooth muscle cells were cultured in vitro (see supplementary Figure S4). The results demonstrate that the regulation of TFPI, TF, and TFPI-2 are correlated not only in vivo but also in vitro, suggesting that the coordinated balance in the expression of the TF/TFPI axis is important for homeostasis and in vascular biology generally.

DISCUSSION

The present study demonstrated that TFPI, the primary inhibitor of the TF-induced coagulation pathway, is required for the integrity of endothelium and balanced hemostasis. TFPI deficiency enhanced endothelial permeability in the lung, and facilitated metastasis in a mouse model. The prometastatic phenotype was largely dependent on the changed pulmonary microenvironment and the systemic and/ or local procoagulant state. The findings suggest that
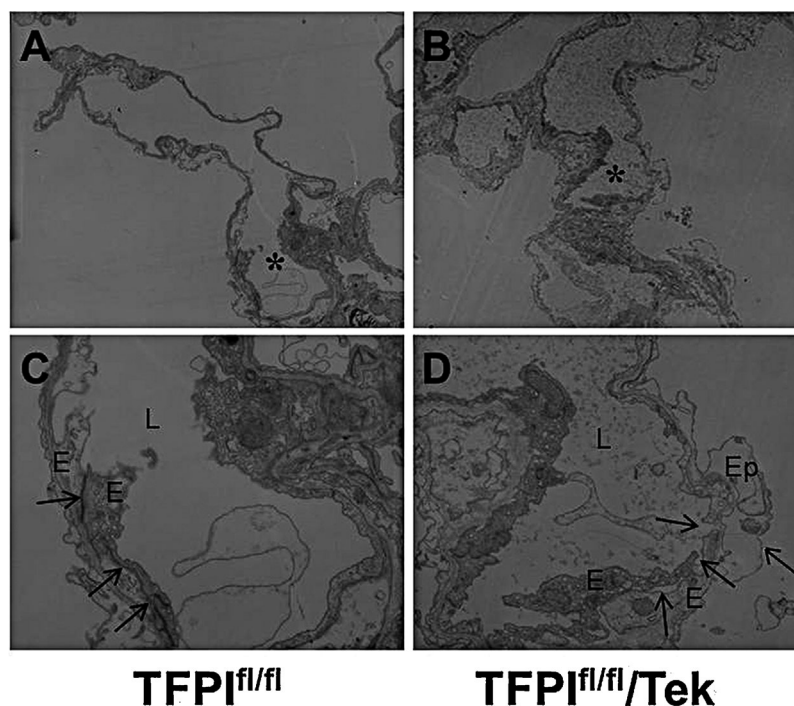
Figure 7. TEM images displayed endothelial cell–cell junctional integrity in the mouse lung. (A, C) The cell–cell junctions of pulmonary endothelial cells of the lungs of TFPI$^{fl/fl}$ ($n = 3$) were tight. (B, D) By contrast, cell–cell junctions appeared to have increased gaps between adjacent cells in the lungs of TFPI$^{fl/fl}$/Tek mice ($n = 4$). *Indicate enlarged areas in A and B. Arrow: cell–cell junctions. L: vascular lumen. E: endothelial cells. Ep: epithelial cells. Red arrow: swollen epithelial cell. Scale bar $= 1 \mu$m (A, B), 2μm (C, D).

the dominant mechanism by which the endothelial cell-anchored TFPI controls the metastatic potential of tumors is predominantly by regulation of local TF-initiated thrombin generation.

To test the hypothesis that endothelial cell-anchored TFPI is a primary determinant of malignancy, we generated mice with the full-length disruption of TFPI (without the KD1, KD2, KD3, and C terminus domains). Studies on *TFPI* gene disruption in mice have shown that systemic homozygotic deletion of KD1 of TFPI results in intrauterine lethality [10,11], which was also observed in TFPI null embryos in our study (see supplemental Figure S1). The intrauterine lethality is likely due to unregulated TF/FVIIa activity
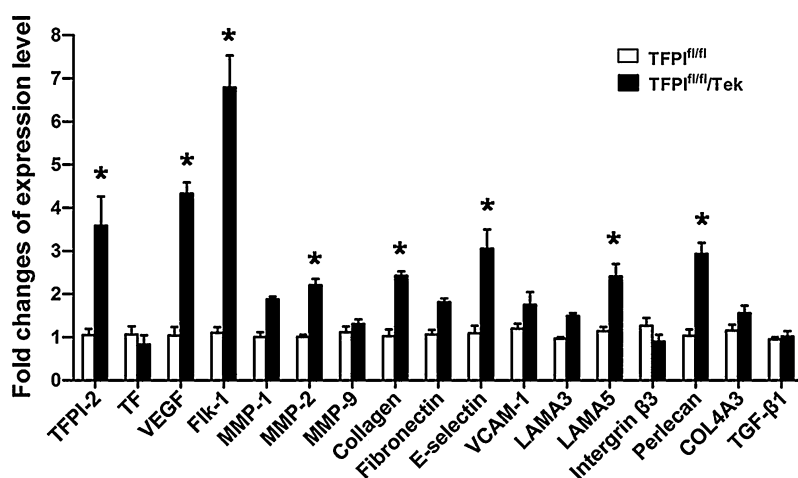

Figure 8. Expression of genes associated with the pro-metastatic phenotype in the lung. (A) qPCR quantified the expression of genes in mouse tissue of the lung . "*" showed a twofold change (or more) with $P < 0.05$. Eight of 16 genes showed a significant increase of more than twofold in the lung of cDNA species of TFPI$^{fl/fl}$/Tek mice vs. TFPI$^{fl/fl}$ mice. These genes included *TFPI-2,VEGF, Flk-1, MMP 2, collagen-1, E-selectin, perlecan*, and *Lama-5*. Data are representative of three independent experiments. Error bars indicate SEM.
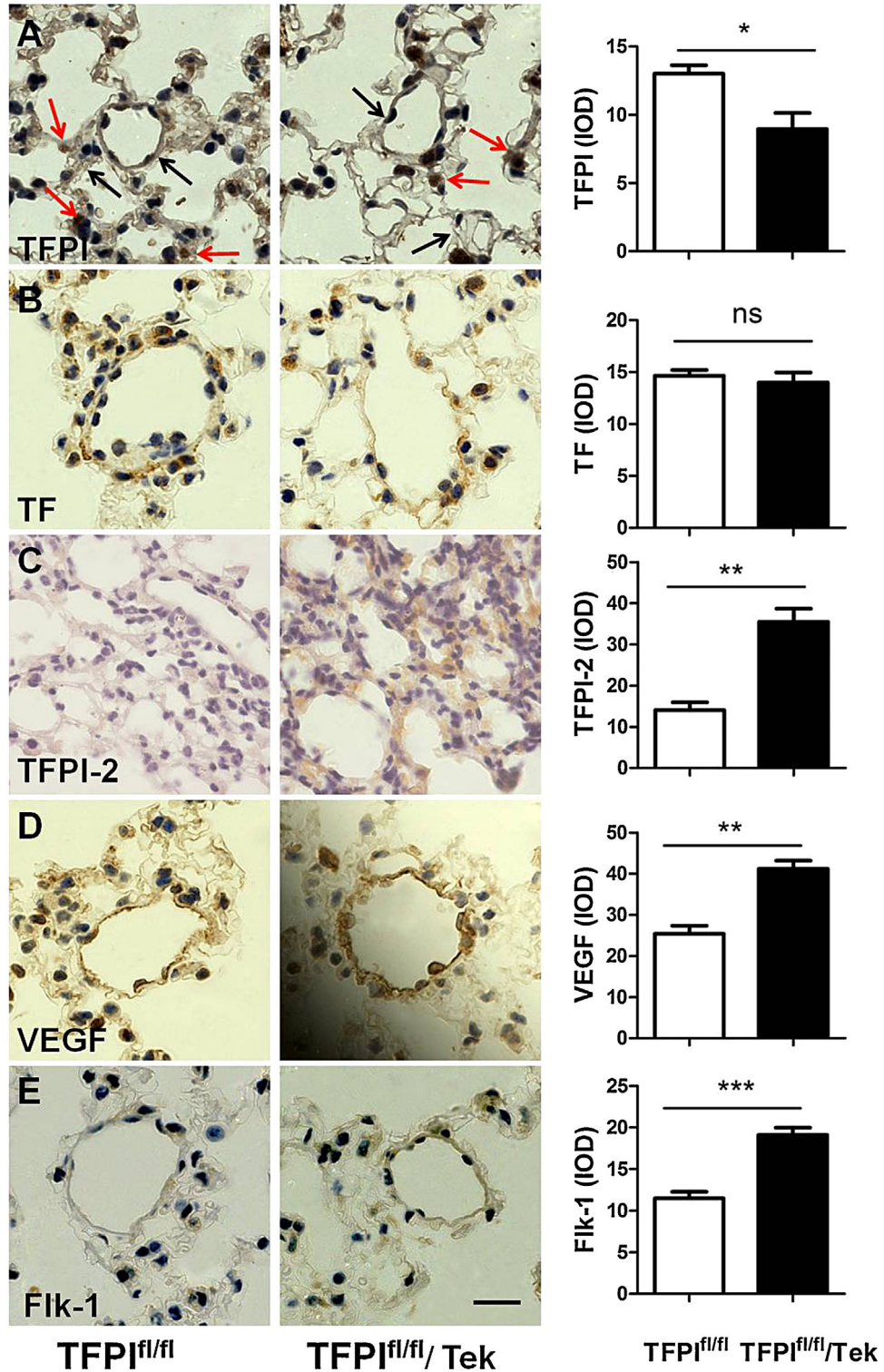
Figure 9. Immunohistochemical analysis of lung sections. TFPI, TF, TFPI-2, VEGF, and Flk-1 of lung tissues were detected by immunohistochemitry staining in TFPI-deficient and control mice. The statistic anyalysis of integrated optical density (IOD) was shown on the right. (A) TFPI knockout in the vascular endothelium did not affect the TFPI expression by alveolar epithelial cell (red arrow), but microvascular endothelia (black arrow) in TFPI-deficient mice demonstrated weaker positive staining than in control mice. (B–E) When TFPI was disrupted in endothelia cells, TF did not show significant difference, whereas TFPI-2, VEGF, and Flk-1 were upregulated, compared with that of the control mice. Data are representative of three independent experiments. $^*P < 0.05$; $^{**}P < 0.01$; $^{***}P < 0.001$. Scale bar $= 20\mu$m. Error bars indicate SEM.

and a consequent consumptive coagulopathy. Disruption of the murine *TF* gene also results in embryonic lethality [36]. TF-null embryos were rescued by expression of low levels of human TF from a transgene expression system [37]. Rescued mice with <1% of wild-type levels have shorter lifespans as compared with control mice, and this is partly due to fatal lung hemorrhage [38]. Extended study showed that low levels of TF rescue TFPI$^{-/-}$ embryos from embryonic lethality, and generates viable adult mice, and does not affect uterine hemostasis or cardiac fibrosis. These results indicate that the correct homeostatic TF/TFPI balance is essential for embryonic development and hemostasis in adult mice [39]. In addition, low-level FVII deficiency also rescued the embryonic lethality of TFPI homogenous embryos. However, neonates died shortly after birth due to FVII deficiency [40], suggesting that the physiological role of TFPI is predominantly associated with TF/FVIIa activity.

One potential mechanism by which TFPI deficiency could support tumor metastasis is by increased generation of TF-initiated thrombin synthesis. Our blood analysis studies and tests of tail bleeding time pointed out no difference between TFPI$^{fl/fl}$/Tek mice and their control littermates, with the notable exception of fibrinogen (Fg). The 28% decrease of Fg (Figure 4B; 0 h) reflected the increased thrombin activity and/or over-activation of fibrinolysis [41]. The increased thrombin activity was confirmed by a 49.4% increase of TAT (Fgiure 4A; 0 h). Combined with the observation that the plasma TFPI concentration of TFPI$^{fl/fl}$/Tek mice was 40.2% lower than that of controls, the hemostasis in the TFPI-deficient mice was altered to a prothrombotic phenotype. The prothrombotic state observed in the TFPI$^{fl/fl}$/Tek mice was similar to other anti-coagulant deficient mice. Thrombomodulin (TM)-deficient mice (TM^{Pro}) expressing a mutant form of TM that reduces both thrombin binding affinity and thrombin-mediated protein C activation, was associated with increased intravascular fibrin deposition, and yet remained free from overt thrombosis [42]. Studies in mice with a severe deficiency in Protein C (1–18% of normal controls) displayed a prothrombotic and proinflammatory phenotype [43]. TFPI-deficient mice exhibited a normal life span, were fertile, and we did not find any evidence of fibrin deposition in organs by light microscopy. These findings indicate that the anti-coagulant deficiency causes a similar phenotype, but the severity might be different. TFPI, TM, and Protein C regulate the TF/Thrombin coagulation axis at different phases of activation. For example, TFPI is responsive to the inhibition of the initiating phase by regulating TF/FVIIa and prothrombinase activity, which blocks thrombin generation. Thrombin involvement in cancer biology is well documented. Thrombin-activated tumor cells enhance adhesion to platelets, and endothelial cells [44,45]. Thrombin

enhances tumor cell development and metastasis, cell growth and angiogenesis [46]. Experimental pulmonary metastasis is promoted by the thrombin-activated PAR-1 pathway in tumor cells [47]. Therefore, unfettered thrombin activity in TFPI$^{fl/fl}$/Tek mice may facilitate tumor metastasis, as seen in TM^{Pro} mice [48,49]. However, the low plasma levels of TFPI found in abetalipoproteinemic patients are due to a lack of low density lipoprotein (LDL), a carrier of TFPI, and yet show similar total TFPI levels in the plasma as do normal individuals after heparin infusion. These patients do not appear to have an increased risk of thrombosis, suggesting that anchored TFPI plays an important role in the regulation of hemostasis [50] and cancer progression. Our data on Plasma TAT, fibrinogen levels and platelet count before and after tumor cell injection, and the rescue experiment with the recombinant adenovirus AdTFPI indicate that TFPI has significant anti-metastatic activity and may do so by regulating tumor cell-induced TF-mediated coagulation activation.

Increased thrombin activity and fibrinolysis in TFPI$^{fl/fl}$/Tek mice would be expected to alter or disrupt the endothelial barrier function, considering that most of the TFPI is positioned on the surface of endothelial cells. Increased vascular permeability drives inflammatory cell infiltration, tumor cell extravasation, and angiogenesis [51]. The finding that the pulmonary microvascular permeability of TFPI$^{fl/fl}$/Tek mice was 34% higher than control littermates indicates that vascular endothelia were injured. This abnormality was confirmed by transmission electron microscopy with defects in cell–cell junctions. Additionally, 16% of endothelial cells were swollen, or adhered to the platelets or neutrophils, suggesting that spontaneous microthrombosis might occur at low levels in the context of unbalanced TF/TFPI activities, and the lung being the second TF-rich tissue in mice [52].

Increased microvascular permeability in the lung might be caused by protease attack. Our data demonstrated that MMP-1, MMP-2, and MMP-9 were upregulated at the mRNA level in the lungs of TFPI$^{fl/fl}$/Tek mice, which suggested the existence of increased fibrinolysis. Plasmin regulates tumor growth and metastasis by the activation of matrix metalloproteases (MMPs). In addition, plasmin can directly break down cell–cell junction proteins like fibronectin, leading to a defect in cell–cell junction or increased microvascular permeability. Interestingly, we observed that TFPI knockout in vascular smooth muscle cells in TFPI$^{fl/fl}$/SMA mice was also accompanied by decreased TF mRNA levels with upregulated TFPI-2, a homolog of TFPI (see supplementary Figure S4). TFPI-2 serves as a plasmin inhibitor, and thus, plays a major role in endothelial cell matrix (ECM) degradation and remodeling by preventing activation of MMPs. Enhanced expression of TFPI-2 might represent a key compensatory mechanism in

the deficiency of TFPI. These data suggest an inhibitory role of TFPI for plasmin in vivo, although controversial results were reported. Some data showed TFPI having a weak inhibitory effect on plasmin [53,54]. A few findings revealed that at high concentrations of plasmin, degradation of TFPI on the cell surface in vitro was possible [55,56].

TF antigen expression was confirmed by immunohistochemistry, and TF levels showed not signifcant difference in the TFPI^{fl/fl}/Tek mice as compared with their control littermates. However, the mRNA levels of TF were down-regulated. We observed down-regulation of TF at the mRNA level in our TFPI knockouts of vascular smooth muscle cells, wherein TF was down-regulated by as much as 80% of the control levels in parallel with TFPI disruption (see supplementary Figure S4). This emphasizes the importance of TF/TFPI balance in vascular biology. Exacerbated TF expression will promote a prometastatic microenvironment in the lung, and will do so via protease-activated receptors (PARs), which are activated by TF or the thrombin signaling pathway. Previous studies have shown that endogenous and recombinant TFPI regulate TF-induced PAR1, and PAR2 signaling pathways, supporting its dual inhibitory functions on the TF-triggered coagulation pathway and TF-dependent signaling activity [57].

Another mechanism that might facilitate pulmonary metastasis is through enhanced VEGF signaling pathways, which is a key regulator of vascular permeability in health and disease. Our data demonstrated that VEGF and Flk-1 (VEGFR2) were elevated at both the mRNA and protein levels, which when combined with other upregulated extracellular matrix proteins, like E-selectin and perlecan suggest that TFPI deficiency in endothelial cells changes the lung microenviroment to a prometastatic phenotype.

Our data also show that under baseline conditions, Evan's blue staining of the brain of TFPI-deficient mice had no significant difference as compared with the control mice. Nevertheless, when lipopolysaccharide (LPS) was used to challenge mice with Evan's blue stain simultaneously, the brain microvascular permeability of TFPI^{fl/fl}/Tek mice showed a 60% higher effect than did TFPI^{fl/fl} mice (see supplementary Figure S2). This suggested that TFPI is less important in this organ, but it might play a key role in the brain certain pathological conditions (e.g., inflammation or sepsis). Vascular endothelium in different organs is made up of phenotypically diverse groups of cells with expression of specific sets of genes that facilitate tissue-specific functions [58–60]. Given that the brain displays a high level of TF but very low TFPI [52], it is reasonable to see the different responses in the mouse model of Evan's blue dye extravasation. By contrast, the heart, expressing intermediate levels of TF, and TFPI, did not show any defects. This is possible since a 52% decrease in the relative mRNA levels is insufficient to significantly change the local balance of TF/

TFPI, and indicates a compensative mechanism is likely from the SMC or cardiomyocyte-derived TFPI.

These findings suggest that TFPI functions in a tissue-specific manner, and a certain critical level of anchored TFPI on endothelial cells, are sufficient to help maintain the integrity of the local vasculature and contribute to a balanced systemic hemostatic response, and in the control of tumor metastasis. It is important to note that endothelial-associated thrombomodulin and circulating protein C might offer an additional compensatory mechanism to maintain and restore adequate hemostasis in a tissue-specific manner, or systemically in TFPI-deficient mice [61].

From the above discussion, we conclude that anchored TFPI maintains the integrity of endothelial cells and to a local and systemic balance in hemostasis. TFPI controls tumor metastasis largely through regulated generation of TF-induced thrombin in a tissue-specific manner. Finally, it is important to note that both TFPIα and TFPIβ isoforms were knocked down in the knockout mice used. Further study should be performed to investigate the functional differences between the two variants in physiology and cancer biology.

REFERENCES

1. Broze GJ, Jr. Tissue factor pathway inhibitor and the current concept of blood coagulation. Blood Coagul Fibrinolysis 1995;6 Suppl 1:S7–S13.

2. Piro O, Broze GJ, Jr. Role for the Kunitz-3 domain of tissue factor pathway inhibitor-alpha in cell surface binding. Circulation 2004;110:3567–3572.

3. Ahnstrom J, Andersson HM, Hockey V, et al. Identification of functionally important residues in TFPI Kunitz domain 3 required for the enhancement of its activity by protein S. Blood 2012;120:5059–5062.

4. Wood JP, Ellery PE, Maroney SA, Mast AE. Protein S is a cofactor for platelet and endothelial tissue factor pathway inhibitor-alpha but not for cell surface-associated tissue factor pathway inhibitor. Arterioscler Thromb Vasc Biol 2014;34:169–176.

5. Piro O, Broze GJ, Jr. Comparison of cell-surface TFPIalpha and beta. J Thromb Haemost 2005;3:2677–2683.

6. Girard TJ, Tuley E, Broze GJ, Jr. TFPIbeta is the GPI-anchored TFPI isoform on human endothelial cells and placental microsomes. Blood 2012;119:1256–1262.

7. Provencal M, Michaud M, Beaulieu E, et al. Tissue factor pathway inhibitor (TFPI) interferes with endothelial cell migration by inhibition of both the Erk pathway and focal adhesion proteins. Thromb Haemost 2008;99:576–585.

8. Hembrough TA, Ruiz JF, Swerdlow BM, et al. Identification and characterization of a very low density lipoprotein receptor-binding peptide from tissue factor pathway inhibitor that has antitumor and antiangiogenic activity. Blood 2004;103:3374–3380.

9. Papareddy P, Kalle M, Kasetty G, et al. C-terminal peptides of tissue factor pathway inhibitor are novel host defense molecules. J Bio Chem 2010;285:28387–28398.

10. Broze GJ, Jr. Tissue factor pathway inhibitor gene disruption. Blood Coagul Fibrinolysis 1998;Suppl 1:S89–S92.

11. White TA, Johnson T, Zarzhevsky N, et al. Endothelial-derived tissue factor pathway inhibitor regulates arterial thrombosis but is not required for development or hemostasis. Blood 2010;116:1787–1794.

12. Zhang J, Piro O, Lu L, Broze GJ, Jr. Glycosyl phosphatidyli-nositol anchorage of tissue factor pathway inhibitor. Circula-tion 2003;108:623–627.

13. Maroney SA, Ellery PE, Wood JP, Ferrel JP, Martinez ND, Mast. AE. Comparison of the inhibitory activities of human tissue factor pathway inhibitor (TFPI) alpha and TFPIbeta. J Thromb Haemost 2013;11:911–918.

14. Kopp CW, Holzenbein T, Steiner S. Inhibition of restenosis by tissue factor pathway inhibitor: In vivo and in vitro evidence for suppressed monocyte chemoattraction and reduced gelatinolytic activity. Blood 2004;103:1653–1661.

15. Pan S, White TA, Witt TA, Chiriac A, Mueske CS, Simari. RD. Vascular-directed tissue factor pathway inhibitor overexpres-sion regulates plasma cholesterol and reduces atherosclerotic plaque development. Circ Res 2009;105:713–720, 718 p following 720.

16. Hamada K, Kuratsu J, Saitoh Y, Takeshima H, Nishi T, Ushio. Y. Expression of tissue factor in glioma. Noshuyo byori = Brain Tumor Pathol 1996;13:115–118.

17. Sawada M, Miyake S, Ohdama S, et al. Expression of tissue factor in non-small-cell lung cancers and its relationship to metastasis. Br J Cancer 1999;79:472–477.

18. Ueda C, Hirohata Y, Kihara Y, et al. Pancreatic cancer complicated by disseminated intravascular coagulation asso-ciated with production of tissue factor. J Gastroenterol 2001;36:848–850.

19. Yu JL, May L, Lhotak V, et al. Oncogenic events regulate tissue factor expression in colorectal cancer cells: Implications for tumor progression and angiogenesis. Blood 2005;105:1734–1741.

20. Cocco E, Varughese J, Buza N, et al. Tissue factor expression in ovarian cancer: Implications for immunotherapy with hI-con1, a factor VII-IgGF(c) chimeric protein targeting tissue factor. Clin Exp Metastasis 2011;28:689–700.

21. Guan M, Jin J, Su B, Liu WW, Lu Y. Tissue factor expression and angiogenesis in human glioma. Clin Biochem 2002;35:321–325.

22. Hembrough TA, Swartz GM, Papathanassiu A, et al. Tissue factor/factor VIIa inhibitors block angiogenesis and tumor growth through a nonhemostatic mechanism. Cancer Res 2003;63:2997–3000.

23. Stavik B, Skretting G, Sletten M, Sandset PM, Iversen. N. Overexpression of both TFPIalpha and TFPIbeta induces apoptosis and expression of genes involved in the death receptor pathway in breast cancer cells. Mol Carcinog 2010;49:951–963.

24. Stavik B, Skretting G, Aasheim HC, et al. Downregulation of TFPI in breast cancer cells induces tyrosine phosphorylation signaling and increases metastatic growth by stimulating cell motility. BMC Cancer 2011;11:357.

25. Amirkhosravi A, Meyer T, Chang JY, et al. Tissue factor pathway inhibitor reduces experimental lung metastasis of B16 melanoma. Thromb Haemost 2002;87:930–936.

26. Sierko E, Wojtukiewicz MZ, Zimnoch L, Kisiel. W. Expression of tissue factor pathway inhibitor (TFPI) in human breast and colon cancer tissue. Thromb Haemost 2010;103:198–204.

27. Kurer MA. Protein and mRNA expression of tissue factor pathway inhibitor-1 (TFPI-1) in breast, pancreatic and colorectal cancer cells. Mol Biol Rep 2007;34:221–224.

28. Qu S, Rinehart C, Wu HH, et al. Gene targeting of ErbB3 using a Cre-mediated unidirectional DNA inversion strategy. Genesis (New York, NY: 2000) 2006;44:477–486.

29. Cotta-de-Almeida V, Schonhoff S, Shibata T, Leiter A, Snapper. SB. A new method for rapidly generating gene-targeting vectors by engineering BACs through homologous recombination in bacteria. Genome Res 2003;13:2190–2194.

30. Zhang Z, Lutz. B. Cre recombinase-mediated inversion using lox66 and lox71: Method to introduce conditional point mutations into the CREB-binding protein. Nucleic Acids Res 2002;30:e90.

31. Koni PA, Joshi SK, Temann UA, Olson D, Burkly L, Flavell. RA. Conditional vascular cell adhesion molecule 1 deletion in mice: Impaired lymphocyte migration to bone marrow. J Exp Med 2001;193:741–754.

32. Agbor LN, Elased KM, Walker. MK. Endothelial cell-specific aryl hydrocarbon receptor knockout mice exhibit hypotension mediated, in part, by an attenuated angiotensin II responsive-ness. Biochem Pharmacol 2011;82:514–523.

33. Overwijk WW, Restifo NP. B16 as a mouse model for human melanoma. Current protocols in immunology/edited by John E. Coligan [et al.] 2001; Chapter 20:Unit 20. 21.

34. Xu Y, Liu YJ, Yu. Q. Angiopoietin-3 inhibits pulmonary metastasis by inhibiting tumor angiogenesis. Cancer Res 2004;64:6119–6126.

35. Wolf MJ, Hoos A, Bauer J, et al. Endothelial CCR2 signaling induced by colon carcinoma cells enables extravasation via the JAK2-Stat5 and p38MAPK pathway. Cancer Cell 2012;22:91–105.

36. Toomey JR, Kratzer KE, Lasky NM, Stanton JJ, Broze GJ, Jr. Targeted disruption of the murine tissue factor gene results in embryonic lethality. Blood 1996;88:1583–1587.

37. Parry GC, Erlich JH, Carmeliet P, Luther T, Mackman. N. Low levels of tissue factor are compatible with development and hemostasis in mice. J Clin Invest 1998;101:560–569.

38. Pawlinski R, Fernandes A, Kehrle B, et al. Tissue factor deficiency causes cardiac fibrosis and left ventricular dysfunc-tion. Proc Natl Acad Sci USA 2002;99:15333–15338.

39. Pedersen B, Holscher T, Sato Y, Pawlinski R, Mackman. N. A balance between tissue factor and tissue factor pathway inhibitor is required for embryonic development and hemo-stasis in adult mice. Blood 2005;105:2777–2782.

40. Chan JC, Carmeliet P, Moons L, et al. Factor VII deficiency rescues the intrauterine lethality in mice associated with a tissue factor pathway inhibitor deficit. J Clin Invest 1999;103:475–482.

41. Sobel JH, Trakht I, Pileggi N, Qi Wu H. Antipeptide monoclonal antibodies to defined fibrinogen Aalpha chain regions: Anti-Aalpha 487-498, a structural probe for fibrinogenolysis. Blood 1998;91:1590–1598.

42. Weiler-Guettler H, Christie PD, Beeler DL, et al. A targeted point mutation in thrombomodulin generates viable mice with a prethrombotic state. J Clin Invest 1998;101:1983–1991.

43. Lay AJ, Liang Z, Rosen ED, Castellino. FJ. Mice with a severe deficiency in protein C display prothrombotic and proin-flammatory phenotypes and compromised maternal repro-ductive capabilities. J Clin Invest 2005;115:1552–1561.

44. Helland IB, Klementsen B, Jorgensen. L. Addition of both platelets and thrombin in combination accelerates tumor cells to adhere to endothelial cells in vitro. In Vitro Cell Dev Biol Anim 1997;33:182–186.

45. Nierodzik ML, Plotkin A, Kajumo F, Karpatkin. S. Thrombin stimulates tumor-platelet adhesion in vitro and metastasis in vivo. J Clin Invest 1991;87:229–236.

46. Hu L, Lee M, Campbell W, Perez-Soler R, Karpatkin. S. Role of endogenous thrombin in tumor implantation, seeding, and spontaneous metastasis. Blood 2004;104:2746–2751.

47. Nierodzik ML, Chen K, Takeshita K, et al. Protease-activated receptor 1 (PAR-1) is required and rate-limiting for thrombin-enhanced experimental pulmonary metastasis. Blood 1998;92:3694–3700.

48. Yokota N, Zarpellon A, Chakrabarty S, et al. Contributions of thrombin targets to tissue factor-dependent metastasis in hyperthrombotic mice. J Thromb Haemost 2014;12:71–81.

49. Horowitz NA, Blevins EA, Miller WM, et al. Thrombomodulin is a determinant of metastasis through a mechanism linked to the thrombin binding domain but not the lectin-like domain. Blood 2011;118:2889–2895.

50. Novotny WF, Brown SG, Miletich JP, Rader DJ, Broze GJ, Jr. Plasma antigen levels of the lipoprotein-associated coagula-tion inhibitor in patient samples. Blood 1991;78:387–393.

51. Harmey JH, Bucana CD, Lu W, et al. Lipopolysaccharide-induced metastatic growth is associated with increased angiogenesis, vascular permeability and tumor cell invasion. Int J Cancer 2002;101:415–422.
52. Welch AJ, Motamedi M, Rastegar S, LeCarpentier GL, Jansen. D. Laser thermal ablation. Photochem Photobiol 1991;53: 815–823.
53. Petersen LC, Bjorn SE, Olsen OH, Nordfang O, Norris F, Norris. K. Inhibitory properties of separate recombinant Kunitz-type-protease-inhibitor domains from tissue-factor-pathway inhibitor. Eur J Biochem 1996;235:310–316.
54. Broze GJ, Jr., Miletich JP. Characterization of the inhibition of tissue factor in serum. Blood 1987;69:150–155.
55. Li A, Wun. TC. Proteolysis of tissue factor pathway inhibitor (TFPI) by plasmin: Effect on TFPI activity. Thromb Haemost 1998;80:423–427.
56. Stalboerger PG, Panetta CJ, Simari RD, Caplice NM. Plasmin proteolysis of endothelial cell and vessel wall associated tissue factor pathway inhibitor. Thromb Haemost 2001;86: 923–928.
57. Ahamed J, Belting M, Ruf. W. Regulation of tissue factor-induced signaling by endogenous and recombinant tissue factor pathway inhibitor 1. Blood 2005;105:2384–2391.
58. Minami T, Aird WC. Endothelial cell gene regulation. Trends Cardiovasc Med 2005;15:174–184.
59. Aird WC. Phenotypic heterogeneity of the endothelium: II. Representative vascular beds. Circ Res 2007;100:174–190.
60. Aird WC. Phenotypic heterogeneity of the endothelium: I. Structure, function, and mechanisms. Circ Res 2007;100: 158–173.
61. Maroney SA, Cooley BC, Sood R, Weiler H, Mast AE. Combined tissue factor pathway inhibitor and thrombomodulin deficiency produces an augmented hypercoagulable state with tissue-specific fibrin deposition. J Thromb Haemost 2008;6:111–117.

SUPPORTING INFORMATION

Additional supporting information may be found in the online version of this article at the publisher's web-site.